Meteoritics & Planetary Science 38, Nr 3, 407–417 (2003)
Abstract available online at http://meteoritics.org

Fassaites in compact type A Ca-Al-rich inclusions in the Ningqiang carbonaceous chondrite: Evidence for partial melting in the nebula

Yangting LIN,[1*] Makoto KIMURA,[2] and Daode WANG[1]

[1]Guangzhou Institute of Geochemistry, Chinese Academy of Sciences, P.O. Box 1131, Guangzhou 510640, China
[2]Institute of Astrophysics & Planetary Science, Ibaraki University, Mito 310, Japan
[*]Corresponding author. E-mail: linyt@gig.ac.cn

(Received 18 June 2002; revision accepted 6 December 2002)

Abstract–Fassaite is a major component of Ca-Al-rich inclusions (CAIs) of Types B and C that crystallized from liquids. In contrast, this mineral is rarely reported in Type A inclusions and has been much less studied. In this paper, we report highly Ti-, Al-enriched fassaite that occurs as rims on perovskite in two compact Type A inclusions from the Ningqiang meteorite. In addition, one of the inclusions contains an euhedral grain of Sc-fassaite (16.4 wt% Sc_2O_3) isolated in melilite. The occurrence and mineral chemistry of the fassaite rims can be explained by a reaction of pre-existing perovskite with CAI melts. Hence, such rims may serve as an indicator for partial melting of Type A inclusions. The Sc-fassaite is probably a relict grain. A third spherical CAI contains several euhedral grains of V-fassaite (4.8–5.4 wt% V_2O_3) enclosed in a melilite fragment. The high V content of fassaite cannot be related to any Fremdlinge, magnetite, or metallic Fe-Ni, because these phases are absent in the inclusion. In the same CAI, other fassaites intergrow with spinel and minor perovskite, filling voids inside of the melilite and space adjacent to the Wark-Lovering rim. The fassaite intergrown with spinel is almost V-free. The coexistence of two types of fassaite suggests that this CAI has not been completely melted.

INTRODUCTION

Some melilite-spinel-rich (Type A) inclusions show compact textures and are referred to as compact Type A (CTA) in contrast to their fluffy counterpart (FTA) (MacPherson and Grossman 1984). Highly irregular shapes, loosely packed textures, gehlenitic melilite, and textural relationships of FTAs are consistent with vapor-solid condensation (MacPherson and Grossman 1984). However, the origin of CTAs is controversial. Although many CTAs show features of crystallization from liquids (e.g., rounded and smooth shapes, radially oriented melilite laths at the inclusion rims, mineral sequence, and REE patterns of major components that are consistent with fractional crystallization), others have irregular shapes and no evidence for a liquid origin (Simon, Davis, and Grossman 1999). Fassaite, an Al-Ti-rich Ca-pyroxene, is one of the most common minerals of Ca-Al-rich inclusions (CAIs). Its modal abundance, occurrence, and mineral chemistry can be related to the different petrographic types of CAIs. Thus, fassaite may provide new hints for the origins of CTAs.

Fassaites from melilite-spinel-fassaite-rich (Type B) and plagioclase-fassaite-rich (Type C) inclusions are most extensively studied. The TiO_2 (referred to as Ti^{4+}) and Al_2O_3 contents usually show a positive correlation, and the former varies from 3 wt% up to 11wt% (Grossman 1975; Wark and Lovering 1982; Wark 1987; Simon, Grossman, and Davis 1991). These fassaites are proposed to crystallize from melts, based on their textural relationships, mineral chemistry, and synthesis experiments (MacPherson and Grossman 1981; Stolper 1982; Stolper and Paque 1986; Simon, Grossman, and Davis 1991). A few Type B inclusions contain fassaites with higher TiO_2 (11–19 wt%) and distinct occurrences from subliquidus grains in the same CAIs, e.g., the bright fringes of fassaite in NQJ331 and NQJ354 from Ningqiang (Lin and Kimura 2000) and the grains enclosed in the melilite mantle of TS34 from Allende (Simon, Grossman, and Davis 1991). These highly Ti-enriched fassaites are possible relict grains in Type Bs (Simon, Grossman, and Davis 1991; Lin and Kimura 2000).

In contrast, fassaite is a minor phase in melilite-spinel-rich (Type A) inclusions, but it contains much higher TiO_2 (14–19 wt%) (Fuchs 1971; Meeker, Wasserburg, and Armstrong 1983; Bischoff and Palme 1987; Podosek et al. 1991; Sylvester, Simon, and Grossman 1993; Simon, Davis, and Grossman 1999; Nazarov, Patchen, and Taylor 2000) than its counterpart in Type B and C inclusions. Most of the

fassaite-bearing Type A inclusions belong to the compact group, i.e., CTA. Consistent with the rounded, smooth shapes and compact textures of many CTAs, these fassaites are reported to have REE patterns that can be predicted by fractional crystallization of liquids (e.g., TS68, Ef3 and A37, Simon, Davis, and Grossman 1999). However, Fassaite REE patterns in other CTAs cannot be explained by any fractional crystallization models. Some of them may be relict grains (e.g., TS32, Simon, Davis, and Grossman 1999) and others, such as fine-grained fassaite together with spinel and perovskite enclosed in melilite probably formed by exsolution of early-crystallized nonstoichiometric melilite (Simon, Davis, and Grossman 1998). In addition, Ti-rich fassaite rims on ragged grains of perovskite have also been reported in a CTA (L1) from Leoville (Sylvester, Simon, and Grossman 1993). However, the origin of the fassaite rims has not been yet clarified.

Sc- and V-rich fassaites have also been found. Almost all reported Sc-rich fassaites (3–18.3 wt% Sc_2O_3) are from ultrarefractory CAIs such as OSCAR (Davis 1984), Essebi-2 (El Goresy et al. 1984), HIB-11 (Simon, Davis, and Grossman 1996), and Efremovka 101.1 (El Goresy et al. 2002), except for E2, a CTA from Efremovka (Ulyanov et al. 1982). Sc-fassaite may have crystallized from liquids produced by melting ultrarefractory precursors. Alternatively, the Sc-enrichment could be related to partitioning with perovskite. V-fassaite (up to 4–6wt% V_2O_3) has been found only in White Angel (a wollastonite-bearing inclusion), Egg-6 (a Type B inclusion from Allende), and some of the above mentioned ultrarefractory CAIs (Meeker, Wasserburg, and Armstrong 1983; Bischoff and Palme 1987; Caillet and Buseck 1992; El Goresy et al. 2002). A common feature of V-fassaite is that it usually coexists with Fe-Ni metals or Fremdlinge.

Here, we report the occurrence of highly Ti-, Al-rich fassaite in two CTAs and V-fassaite in another spherical CAI from the Ningqiang carbonaceous chondrite. In addition, one of the CTAs contains a grain of fassaite with the second highest Sc_2O_3 content analyzed to date. The origins of these fassaites and their host CAIs are discussed based on petrography and mineral chemistry. The Ningqiang meteorite is an anomalous CV or CK chondrite (Rubin et al. 1988; Kallemeyn, Rubin, and Wasson 1991; Kallemeyn 1996; Kimura et al. 1997) and contains all types of CAIs common in CV3 chondrites (Lin, Kimura, and Wang 1996; Lin and Kimura 1997, 1998, 2000, 2003). Preliminary results of this work were reported by Lin, Kimura, and Wang (1996).

SAMPLES AND EXPERIMENT

Three CAIs, NQW3–9, NQJ3–5–7, and NQW1–20, were found in polished thin sections of NQW3, NQJ3–5, and NQW1, respectively. A JEOL 733 electron microprobe analyzer, equipped with a backscattered electron detector and wavelength dispersive spectrometers, was used for both textural observations and quantitative analyses. The quantitative analyses were done at 20 kV accelerating voltage and 20 nA beam current for analyses of Sc, Zr, Ce and other elements in fassaite and perovskite. The other phases and bulk compositions of the CAIs were analyzed at 15 kV with a beam current of 10 nA. X-ray peak overlapping of Sc by Ca, V by Ti, and Ce by Ti and V was corrected using a deconvolution program. The data were corrected using the Bence-Albee method. The detection limits (1σ) for the focused beam analyses are as follows (in wt%): SiO_2 0.02, TiO_2 0.03, Al_2O_3 0.02, Cr_2O_3 0.03, V_2O_3 0.02, FeO 0.05, MnO 0.06, MgO 0.02, CaO 0.02, ZnO 0.10, Na_2O 0.02, Sc_2O_3 0.01, ZrO_2 0.06, Sm_2O_3 0.04, Ce_2O_3 0.03, and Eu_2O_3 0.04. Modal compositions of the inclusions were calculated from the areas of the individual phases on backscattered electron (BSE) images and bulk compositions were determined using a broad beam (50 μm in diameter for NQW3–9, 20 μm for the other two CAIs) method (Lin and Kimura 1998), ignoring the effects of non-equatorial section planes of concentrically zoned CAIs.

PETROGRAPHY AND MINERALOGY

NQW3–9

This inclusion is referred to as a CTA (5.8 × 3.3 mm) but has an irregular shape. Some parts of the inclusion were lost during section preparation. The remaining areas have an average modal composition of 84.0 vol% melilite, 14.5 vol% spinel, and 1.5 vol% perovskite with minor fassaite and trace anorthite and feldspathoids (Fig. 1a). Melilite has a compact texture consisting of polygonal crystals (10–40 μm). Spinel occurs mainly near the inclusion rim as a discontinuous layer or clusters to form framboids. Some subhedral to euhedral grains of spinel (<15 μm in size) are heterogeneously enclosed in melilite. Perovskite is rounded, with a size up to 25 μm, and is also unevenly enclosed in melilite. A long lump of perovskite (10 × 100 μm) was found near the inclusion rim. A remarkable feature of this CAI is the presence of minor fassaite as rims on perovskite or as irregular grains enclosing perovskite (Figs. 1a and 1b). Both fassaite and perovskite are embedded in melilite. Small grains (<5 μm) of anorthite and feldspathoids (nepheline and sodalite) were found in cracks or voids in melilite and are probably alteration products of melilite. This inclusion has no Wark-Lovering (WL) rim. Instead, the surface of the inclusion consists of fine-grained melilite and spinel. The bulk composition is given in Table 1 and plotted in Fig. 2.

The melilite is gehlenitic ($Åk_{5–14}$) and contains little Na_2O (Table 2). Analyses from the inclusion rim to the core show no systematic variation in composition. Spinels in various occurrences are almost stoichiometric $MgAl_2O_4$ with minor FeO (0.05–0.87 wt%, except for 5 of 28 analyses with a range of 1.30–2.79 wt%), V_2O_3 (0.28–0.66 wt%), and TiO_2 (0.15–0.53 wt%), and no detectable Cr_2O_3. Perovskite

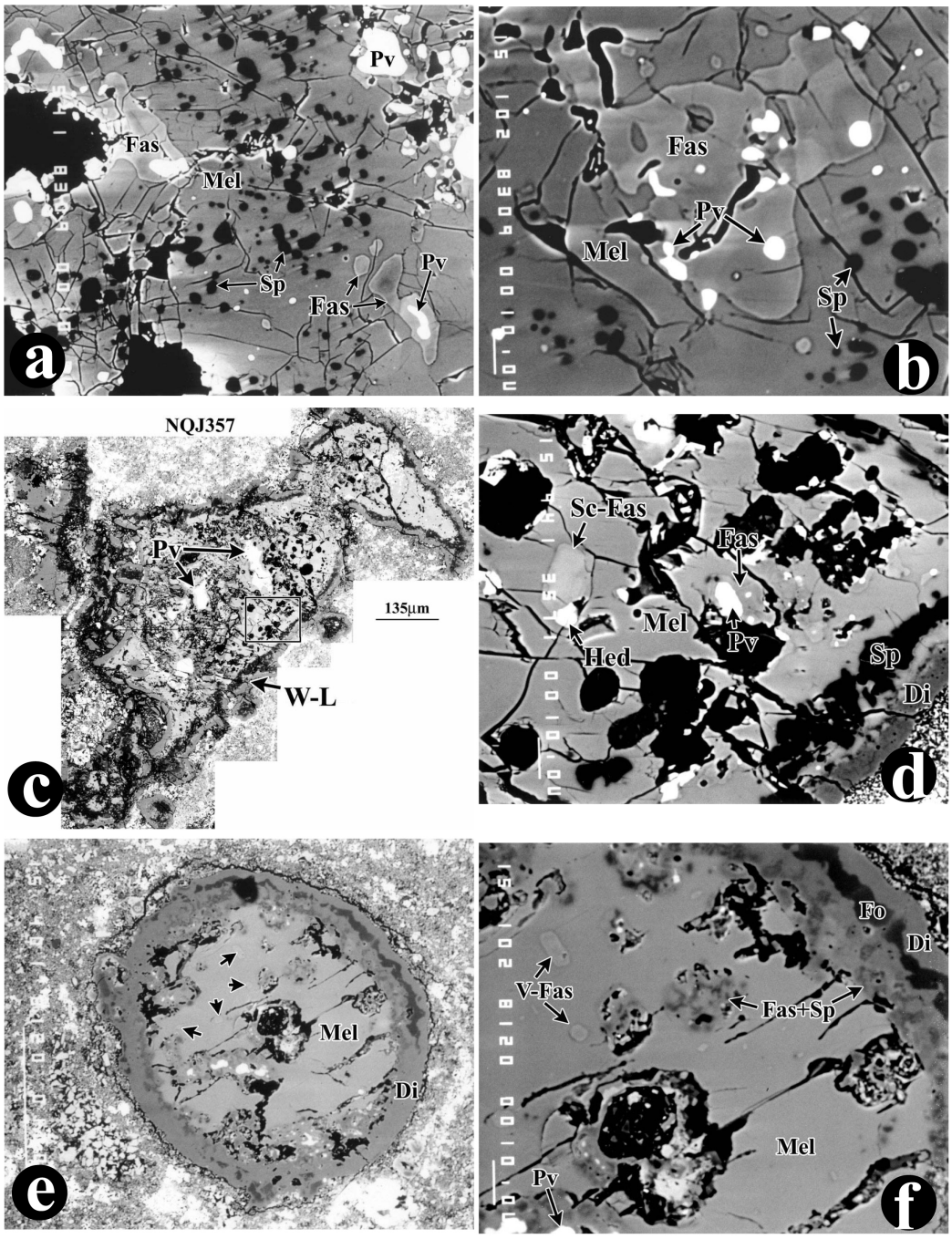

Fig. 1. BSE images of fassaites in Ningqiang CAIs: a) in NQW3–9, fassaite (Fas) occurs as rims on perovskites (Pv), both embedded in melilite (Mel). The dark, euhedral or round grains are spinel (Sp). The field of view is 200 μm; b) in NQW3–9, another anhedral fassaite encloses several rounded grains of perovskite. The field of view is 110 μm; c) NQJ3–5–7 showing its irregular shape, consisting predominantly of melilite rimmed by spinel and diopside layers (Di). Perovskite mainly occurs as lumps in the center of the inclusion. The field of view is 1.0 mm; d) inset of NQJ3–5–7 showing an euhedral grain of Sc-fassaite (Sc-Px) enclosed in melilite. A small, bright grain in contact with the Sc-fassaite is hedenbergite (Hed). Also, note thin fassaite rims around small perovskites. The field of view is 115 μm; e) NQW1–20 has a spherical shape and consists of a melilite core surrounded by a WL rim. Note the ragged shape of the melilite. The fine-grained intergrowth occurs as pockets inside the melilite fragment or filling voids adjacent to the WL rim. The arrows show locations of the V-rich fassaites seen in the next inset figure. The field of view is 270 μm; f) inset of NQW1–20 showing small and euhedral V-rich fassaites enclosed in melilite and the fine-grained intergrowth of fassaite and spinel. The bright grains are perovskite. The WL rim consists of, from inside to out, intergrowths of fassaite and spinel, forsterite, and diopside. The field of view is 110 μm.

Table 1. Bulk compositions of Ningqiang CAIs (normalized to 100 wt%).

	NQW3–9	NQJ3–5–7		NQW1–20	
		1	2[a]	1	2[a]
SiO2	21.3	25.8	24.9	28.3	31.5
TiO_2[b]	1.46	2.11	2.12	2.49	2.16
Al_2O_3	36.4	33.1	34.6	27.5	24.1
Cr_2O_3	0.58	b.d.	b.d.	1.35	1.35
FeO	0.51	1.50	1.99	2.06	3.19
MgO	4.84	5.56	7.81	5.64	9.50
CaO	34.5	30.6	27.3	31.6	27.3
Na_2O	0.14	1.06	0.99	0.87	0.73
P_2O_5	0.18	0.12	b.d.	0.13	b.d.
Cl	b.d.	0.16	0.16	0.15	0.13

[a]Including the WL rim.
[b]As Ti^{4+}; b.d.: below detection limit (1σ, wt%: Cr_2O_3 0.14, P_2O_5 0.08, Cl 0.06.).

contains minor Al_2O_3 (0.15–0.22 wt%), V_2O_3 (0.15–0.28 wt%), ZrO_2 (0.07–0.17 wt%), and Ce_2O_3 (<0.24 wt%) with no detectable Sc_2O_3. The compositions of the fassaites are distinct from those in Types B and C inclusions from Ningqiang (Table 3 and Fig. 3). They are high in TiO_2 (15.8–20.3 wt%), and contain 19.5–26.7 wt% Al_2O_3, 0.32–1.40 wt% V_2O_3, 0.22–0.64 wt% Sc_2O_3, and 0.16–0.19 wt% ZrO_2 with no detectable Ce_2O_3. A $Ti^{3+}/\sum Ti$ ratio of 0.75 ± 0.06 is calculated based on the stoichiometric composition of fassaite, assuming 4 cations per 6 oxygens.

NQJ3–5–7

This inclusion is irregular and has a size of 500 × 1100 μm (Fig. 1c). It is almost completely surrounded by a WL rim consisting of monomineralic layers of, from inside to out, spinel (<20 μm wide), melilite (discontinuous, <5 μm wide) and diopside (5–10 μm wide). A few laths of hibonite are embedded in the spinel layer of the WL rim. In the center of the inclusion, lumps (up to 40 × 120 μm) of perovskite are enclosed in the compact melilite. A euhedral grain of Sc-fassaite (10 × 20 μm) is isolated in melilite, adjacent to a small (5 μm) hedenbergite grain (Fig. 1d). Minor fassaite occurs as thin rims around a few small grains of perovskite at a distance <30 μm from the Sc-fassaite. However, fassaite rims were not found on the large lumps of perovskite in the inclusion center.

Melilite seems to be slightly more gehlenitic ($Åk_{2–6}$) near the rim of the inclusion than in the center ($Åk_{6–10}$). Compared with spinel in NQW3–9, the grains in NQJ3–5–7 contain somewhat higher FeO (0.58–1.77 wt%, except for one analysis of 4.21 wt%) and lower V_2O_3 (0.10–0.30 wt%). Perovskite contains minor Al_2O_3 (0.48–0.61 wt%), V_2O_3 (0.32–0.51

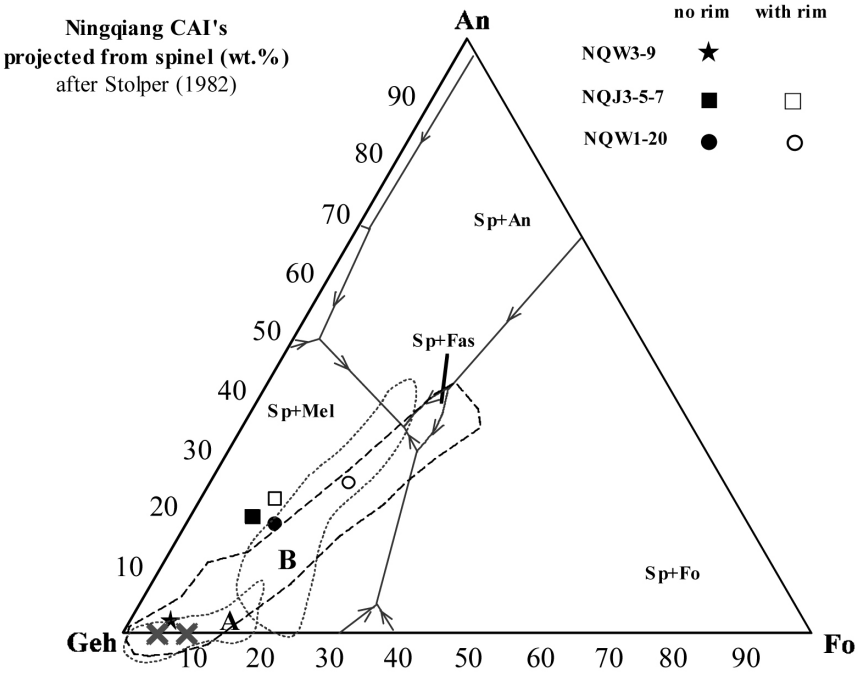

Fig. 2. Bulk compositions of Ningqiang CAIs. The analysis of NQW3–9 plots within the Type A range, while those of NQJ3–5–7 and NQW1–20, both with and without the WL rims are close to or within the range of Type Bs. Cross symbols on gehlenite-forsterite join refer to melilite with $Åk_{10}$ and $Åk_{20}$, respectively. The ranges of Type A and B outlined by dotted lines are after Grossman et al. (2000), and the extended range of Type A outlined by dashed line after Lin and Kimura (2003).

Table 2. Representative compositions of melilite, spinel, and hibonite in Ningqiang CAIs (wt%).

	Melilite						Spinel				Hibonite	
	NQW3–9		NQJ3–5–7		NQW1–20		NQW3–9		NQJ3–5–7		NQJ3–5–7	
SiO_2	24.8	23.3	24.2	22.3	27.1	25.6	b.d.	b.d.	b.d.	b.d.	b.d.	0.27
TiO_2[a]	b.d.	b.d.	0.06	0.13	b.d.	b.d.	0.26	0.15	0.45	0.15	4.63	1.45
Al_2O_3	31.7	34.3	33.6	36.0	28.8	31.2	71.2	70.7	71.8	71.3	85.1	89.3
Cr_2O_3	b.d.	b.d.	0.10	0.12	b.d.	b.d.	b.d.	0.03	0.13	b.d.	b.d.	b.d.
V_2O_3							0.58	0.41	0.10	0.17	0.22	0.11
FeO	b.d.	b.d.	0.13	0.24	b.d.	0.15	0.11	2.79	0.67	0.58	0.24	0.12
MnO	b.d.	b.d.	b.d.	0.07	b.d.	b.d.	b.d.	b.d.	b.d.	b.d.	b.d.	b.d.
MgO	2.08	1.09	1.40	0.24	3.38	2.47	28.3	26.2	28.4	28.5	2.41	1.17
CaO	40.3	40.4	40.8	40.7	40.8	41.0	0.04	0.17	0.25	0.03	8.01	8.35
ZnO							b.d.	b.d.	b.d.	b.d.	b.d.	b.d.
Na_2O	b.d.	0.04	0.05	0.06	0.05	0.06	b.d.	b.d.	b.d.	b.d.	b.d.	b.d.
Total	98.8	99.1	100.4	99.9	100.1	100.4	100.5	100.4	101.8	100.8	100.6	100.8
	Atomic ratios											
Si	1.143	1.070	1.098	1.022	1.232	1.160	0.000	0.000	0.000	0.000	0.000	0.031
Ti	0.000	0.000	0.003	0.004	0.000	0.000	0.005	0.003	0.008	0.003	0.390	0.121
Al	1.721	1.859	1.800	1.940	1.543	1.669	1.984	1.992	1.979	1.984	11.209	11.645
Cr	0.000	0.000	0.003	0.004	0.000	0.000	0.000	0.001	0.003	0.000	0.000	0.000
V							0.011	0.008	0.002	0.003	0.019	0.009
Fe	0.000	0.000	0.005	0.010	0.000	0.006	0.002	0.056	0.013	0.012	0.021	0.012
Mn	0.000	0.000	0.000	0.003	0.000	0.000	0.000	0.000	0.000	0.000	0.000	0.000
Mg	0.144	0.074	0.095	0.017	0.229	0.168	0.995	0.934	0.990	1.003	0.401	0.192
Ca	1.991	1.991	1.990	1.994	1.990	1.993	0.001	0.005	0.007	0.001	0.960	0.989
Zn							0.000	0.000	0.000	0.000	0.000	0.000
Na	0.000	0.004	0.004	0.005	0.004	0.005	0.000	0.000	0.000	0.000	0.000	0.000
Sum	4.999	4.999	4.998	4.999	4.999	5.001	2.997	2.998	3.001	3.004	13.000	13.000
Åk (mol%)	14	7.4	10	2.6	23	17						

[a]As Ti^{4+}

b.d.: below detection limit

Blank space: not analyzed

wt%), Sc_2O_3 (0.14–0.17 wt%), and ZrO_2 (0.06–0.20 wt%). Hibonite contains 1.45–4.89 wt% TiO_2 and 1.17–2.58 wt% MgO with minor V_2O_3 (0.11–0.24 wt%). The Sc-fassaite appears to be zoned, with the core containing higher Sc_2O_3 (15.1–16.4 wt%) than the rim (12.0–12.8 wt%). This is the second highest Sc_2O_3 concentration ever reported in fassaite. The Sc-fassaite also contains high Al_2O_3 (26.0–28.6 wt%), TiO_2 (8.28–10.6 wt%), and V_2O_3 (1.04–1.30 wt%). No ZrO_2 was detected in the core and it is very low at the rim (0.15–0.17 wt%). The calculated Ti^{3+}/Ti ratio of the Sc-fassaite is within the range of the fassaite rims on perovskite in NQJ3–9 (Table 3). The thin fassaite rims on perovskite are TiO_2-rich, similar to those in NQW3–9, but with lower calculated Ti^{3+}/Ti ratios (Table 3). Diopside ($En_{49–52}Wo_{48–51}$) in the WL rim contains 1.68–6.31 wt% Al_2O_3 with minor TiO_2 (0.23–1.11 wt%).

The modal composition of this inclusion is 49.2 vol% melilite, 7.2 vol% perovskite, 10.6 vol% spinel, and 33.0 vol% diopside (all spinel and diopside are from the WL rim) with minor fassaite and a few laths of hibonite. The bulk compositions, with and without the WL rim, are given in Table 1. They plot close to the range of Type B inclusions (Fig. 2). However, this inclusion is surely not Type B. Except for the trace Sc- and/or Ti-rich fassaites, most Ca-pyroxene in NQJ3–5–7 occur as part of the WL rim, distinct from the subliquidus grains in typical Type Bs. No primary anorthite, a common phase in Type Bs, is found in NQJ3–5–7. In addition, the melilite is very gehlenitic ($Geh_{90–98}$) in comparison with the range of Type Bs ($Åk_{15–60}$ for subtype B1, $Åk_{60–85}$ for subtype B2, Wark and Lovering 1982). The range of Type A inclusions outlined in Fig. 2 is based on only a few analyses that are almost all CTAs (Grossman et al. 2000). Our analyses of 107 other CAIs (most are FTAs and spinel-pyroxene inclusions) from Ningqiang reveal there is a continuum in mineralogy and bulk composition between different types of CAIs, and such a continuum is consistent with the condensation origin of these objects (Lin and Kimura 2003). The range of Type A inclusions can be extended to that of Type Bs (Fig. 2). In fact, the inner region of NQJ3–5–7, excluding the WL rim, is typical of Type A inclusions with regard to the predominant and gehlenitic melilite, the high abundance of perovskite, and the absence of subliquidus anorthite and fassaite. Hence we refer to NQJ3–5–7 as a compact Type A.

NQW1–20

This inclusion is a spherule with a diameter of 170 μm

(Fig. 1e). It mainly contains a melilite core and a WL rim (15 μm in width). The WL rim consists of layers of, from inside to out, an intergrowth of Al-rich diopside and spinel, then forsterite, and then diopside (Fig. 1f). The forsterite layer is discontinuous. The melilite is a single crystal with a ragged outline observed under optical microscope. It encloses several small (<10 μm) euhedral grains of V-fassaite (Fig. 1f). Fine-grained intergrowths of fassaite and spinel occur as pockets inside the melilite or fill voids adjacent to the WL rim. They look similar to the innermost layer of the WL rim, except for the occurrence of fine-grained perovskite in the former. Some grains of perovskite have been partially altered to ilmenite. The bulk composition of NQW1–20 plots within both the range of Type Bs and the extended one of Type As (Fig. 2).

The melilite crystal shows a narrow compositional range of $Åk_{15–20}$, except for a few analyses with higher $Åk_{23–25}$ in the center. The Åk content is within the range of fluffy Type A inclusions (MacPherson and Grossman 1984). All small grains of fassaite isolated in the melilite are characteristically V_2O_3-rich (4.76–5.37 wt%), and contain high Al_2O_3 (20.6 wt%) and TiO_2 (14.1–15.0 wt%) with minor Sc_2O_3 (0.33–0.39 wt%) and Cr_2O_3 (0.30–0.45 wt%). No ZrO_2 was detected. The calculated $Ti^{3+}/\sum Ti$ ratios range from 0.67 to 0.84. In contrast, fassaite intergrown with spinel is almost free of V_2O_3, Sc_2O_3, and Cr_2O_3. The contents of Al_2O_3 and TiO_2 are 19.0–23.2 wt% and 13.7–16.3 wt%, respectively. Diopside ($En_{51–52}Wo_{48–49}$) in the WL rim contains <0.5 wt% TiO_2, and the Al_2O_3 content decreases from 8.76 to 1.51 wt% from the inner side outward. Perovskite contains minor V_2O_3 (0.20–0.26 wt%), but no Sc_2O_3 or ZrO_2. Forsterite is nearly pure Mg_2SiO_4 (Fo_{99}) with 0.18 wt% CaO. The petrography and mineral chemistry argue against classification of NQW1–20 as a Type B inclusion. We refer to it as a unique Ca-Al-rich spherule.

Table 3. Representative compositions of perovskite and fassaite in Ningqiang CAIs (wt%).

	Fassaite									Provskite	
	NQW3–9		NQJ3–5–7			NQW1–20				NQW3–9	NQJ3–5–7
	1	2	3	4°	5#	6	7	8	9	10	11
MgO	3.26	4.51	6.11	1.36	2.09	3.56	3.75	6.93	13.1	b.d.	b.d.
CaO	24.3	24.7	27.1	24.6	24.6	24.8	25.3	25.5	24.0	41.2	43.3
Cr_2O_3	0.10	0.06				0.45	0.30	0.08	b.d.	b.d.	
Al_2O_3	24.2	22.3	20.3	21.9	21.3	20.6	20.6	18.9	18.1	0.15	0.41
SiO_2	27.7	30.2	29.6	26.0	27.1	30.3	28.9	32.5	42.8	0.12	0.21
TiO_2[a]	19.5	17.7	18.5	8.28	10.6	14.1	15.0	15.0	2.67	57.7	57.6
MnO	b.d.	b.d.				b.d.	b.d.	b.d.	b.d.	b.d.	
V_2O_3	1.06	0.64	0.11	1.04	1.30	5.37	4.76	0.07	0.04	0.15	0.35
Sc_2O_3	0.64	0.32	0.25	16.4	12.8	0.33	0.39	b.d.		b.d.	0.14
ZrO_2	0.16	0.17	b.d.	b.d.	0.17	b.d.	b.d.	b.d.		0.17	0.06
Ce_2O_3	b.d.	b.d.				b.d.	b.d.	0.05		b.d.	
Sm_2O_3	b.d.	b.d.				b.d.	b.d.	b.d.		b.d.	
Eu_2O_3	b.d.	b.d.				b.d.	b.d.	b.d.		b.d.	
Total	101.0	100.7	102.0	99.6	99.9	99.6	99.0	99.1	100.7	99.4	102.0
						Atomic ratios					
Mg	0.188	0.258	0.344	0.080	0.122	0.208	0.220	0.398	0.701	0.000	0.000
Ca	1.009	1.018	1.098	1.040	1.035	1.043	1.066	1.053	0.923	1.005	1.034
Cr	0.003	0.002				0.014	0.009	0.003	0.000	0.000	
Al	1.105	1.012	0.903	1.015	0.985	0.953	0.958	0.859	0.764	0.004	0.011
Si	1.071	1.163	1.118	1.024	1.062	1.186	1.138	1.251	1.532	0.003	0.005
Ti	0.566	0.513	0.524	0.245	0.314	0.417	0.445	0.434	0.072	0.988	0.963
Mn	0.000	0.000				0.000	0.000	0.000	0.000	0.000	
V	0.033	0.020	0.003	0.033	0.041	0.169	0.150	0.002	0.001	0.003	0.006
Sc	0.022	0.011	0.008	0.562	0.438	0.011	0.013	0.000		0.000	0.003
Zr	0.003	0.003	0.001	0.000	0.003	0.000	0.000	0.000		0.002	0.001
Ce	0.000	0.000				0.000	0.000	0.001		0.000	
Sm	0.000	0.000				0.000	0.000	0.000		0.000	
Eu	0.000	0.000				0.000	0.000	0.000		0.000	
Sum	4.000	4.000	4.000	4.000	4.000	4.000	4.000	4.000	3.993	2.004	2.022
Ti^{3+}/ Ti	0.78	0.79	0.38	0.61	0.70	0.84	0.67	0.54			

[a]As Ti^{4+}

b.d.: below detection limit

blank space: not analyzed

1–3: as rims around perovskite; 4–5: Sc-rich fassaite, #rim, °core; 6–7: enclosed in melilite; 8–9: intergrown with spinel.

DISCUSSION

Significance of Al-Ti-Rich Fassaites

Fassaite Rims on Perovskite

In both CTAs, NQW3–9 and NQJ3–5–7, fassaite occurs as rims around perovskite and contains very high TiO_2, distinct from the Ca-pyroxene in the WL rims of the same inclusions and from subliquidus fassaite grains in Type B and C inclusions. The composition of the fassaite rims is also different from that of the fringes of fassaite found in Type B inclusions from Ningqiang (Fig. 3). The unique occurrence and mineral chemistry of these rims suggest a different origin.

A possible origin of the fassaite rims is reaction of perovskite with CAI melts. This is consistent with their occurrences and high Ti contents. Perovskite grains rimmed by fassaite are usually rounded (Figs. 1a and 1b), suggestive of a reaction with liquid. The same origin has been proposed for fassaite in the ultrarefractory inclusion 101.1 from Efremovka (El Goresy et al. 2002), which shows a similar occurrence as rims on perovskite. These fassaite rims have trace element abundance patterns complementary to that of the coexisting perovskite in terms of subsolidus equilibrium between them (El Goresy et al. 2002). The distinctly higher Sc + Zr contents of the fassaite in 101.1 could be due to the different compositions of the pre-existing perovskites. This is consistent with the ultrarefractory nature of 101.1. Beside the ultrarefractory inclusion 101.1, fassaite rims on perovskite have been observed in compact Type A inclusions E2 from Efremovka (Ulyanov et al. 1982) and L1 from Leoville (Sylvester, Simon, and Grossman 1993). All of these inclusions, including NQW3–9 and NQJ3–5–7, show compact textures, suggesting annealing or melting events in the nebula. On the other hand, the irregular shapes of NQW3–9 and NQJ3–5–7 suggest that the whole inclusions have not been completely melted. We propose that the fassaite rims on perovskite can be referred to as an indicator for partial melting, distinguishing compact Type A inclusions from their fluffy counterparts.

Vapor-solid condensation of the fassaite rims seems unlikely because they were not reported in fluffy Type A inclusions, the most likely condensate assemblages among CAIs (MacPherson and Grossman 1984). Perovskite is a

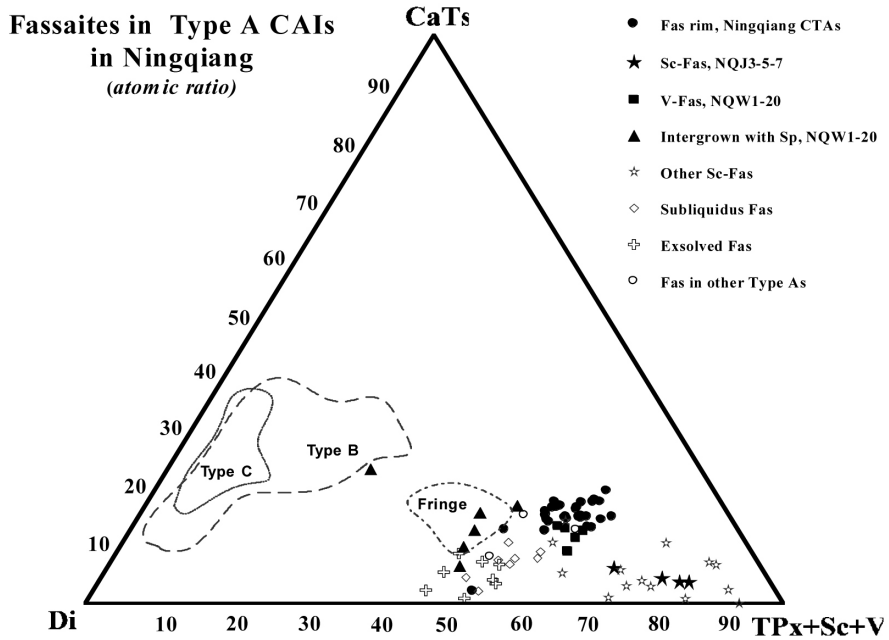

Fig. 3. Compositions of fassaites in Ningqiang Type A inclusions. The fassaite rims on perovskites in Ningqiang CTAs (NQJ3–5–7 and NQW3–9) show compositions distinct from both subliquidus and exsolved grains in other Type As, while the Sc-fassaite in NQJ3–5–7 is within the range of its counterparts in other CAIs. Ranges for fassaites from Types B and C and fringes of fassaite in two Type Bs from Ningqiang are shown for comparison (Lin and Kimura 1998, 2000). A few gains from other Type A inclusions overlap with the fassaite rims and the subsolidus grains, but their origins are not yet clarified. Literature: other Sc-fassaites from Ulyanov et al. (1982), Simon, Davis, and Grossman (1996) and El Goresy et al. (2002), subliquidus fassaites from Bischoff and Palme (1987) and Simon, Davis, and Grossman (1999), exsolved fassaites from Simon, Davis, and Grossman (1998, 1999), and fassaites in other Type As from Fuchs (1971); Meeker, Wasserburg, and Armstrong (1983); and Podosek et al. (1991). Endmember components of the fassaites include diopside, Ca-Tschermak ($CaAl_2SiO_6$), Ti-Pyroxenes ($CaTi^{3+}AlSiO_6 + CaTi^{4+}Al_2O_6$), Sc-Pyroxene ($CaScAlSiO_6$), Zr-Pyroxene ($CaZrAl_2O_6$), and V-pyroxene ($CaVAlSiO_6$).

common minor phase in FTAs but has no fassaite rims. Moreover, the occurrence of the fassaite rims on perovskites enclosed in melilite suggests a formation sequence in order of perovskite, fassaite, and melilite. This is inconsistent with the sequence of condensation in the nebula, because fassaite is expected to condense at ~180 K lower than melilite (Yoneda and Grossman 1995).

Alternatively, the fassaite rims may crystallize from liquids. Ti-rich fassaites have been reported in several other CTAs, e.g., Ef3 (Sylvester, Simon, and Grossman 1993; Simon, Davis, and Grossman 1999), TS68 and A37 (Simon, Davis, and Grossman 1999), and E202 (Nazarov, Patchen, and Taylor 2000). They were proposed to crystallize from residual liquids, based on their textures and REE patterns similar to their counterparts in Type B inclusions (Simon, Davis, and Grossman 1999). However, this origin cannot explain the occurrence of the fassaite rims on perovskite in NQW3–9 and NQJ3–5–7. The fassaite rims and perovskite are enclosed in melilite instead of intergrowth with the latter. Furthermore, the compositions of the fassaite rims in NQW3–9 and NQJ3–5–7 are distinguishable from the subliquidus fassaites in other Type As (except for one analysis within the range of the latter, Fig. 3), suggestive of their different origins. Fassaite rims on perovskite in other Type A inclusions are Sc-rich (see subsection of Sc-rich fassaite), different from the subliquidus fassaite grains. In addition, it is not possible that the fassaite rims formed by exsolution of early-crystallized nonstoichiometric melilite as proposed for Ti-fassaite in TS2 and TS32 CTAs (Simon, Davis, and Grossman 1998), based on their distinct occurrences and mineral chemistries (Fig. 3).

Sc-Rich Fassaite

The Sc-fassaite enclosed in melilite in NQJ3–5–7 contains the second highest Sc_2O_3 reported to date. However, it has no detectable ZrO_2 in the core, giving it the highest Sc_2O_3/ZrO_2 ratio (>16.4/0.06) (Fig. 4). The composition of the Sc-fassaite is clearly distinct from the fassaite rims on perovskites in both NQW3–9 and NQJ3–5–7, which have low Sc_2O_3 contents (<0.64 wt%) and low Sc_2O_3/ZrO_2 ratios (1.2–6.3). Furthermore, the Sc-rich grain is euhedral in shape, and shows no apparent relationship with perovskite in contrast to the fassaite rims. Other highly Sc-enriched fassaites (12–18.3 wt% Sc_2O_3) have been found in three CAIs (OSCAR, HIB-11, and Efremovka 101.1) with ultrarefractory trace element patterns (Davis 1984; Simon, Davis, and Grossman 1996; El Goresy et al. 2002). These Sc-rich fassaites show close spatial relationships with perovskite, e.g., as rims on perovskite in Efremovka 101.1 or as grains enclosing perovskite in the other two inclusions.

It is unlikely that the Sc-fassaite in NQJ3–5–7 formed by a reaction of perovskite with a CAI melt as proposed above for the fassaite rims. The Sc content of perovskite in NQJ3–5–7 (0.14–0.17 wt%) is too low to explain the Sc content of the fassaite. Even in the ultrarefractory inclusions OSCAR, HIB-11, and Efremovka 101.1, no perovskite contains Sc_2O_3 higher than 0.9 wt% (Davis 1984; Simon, Davis, and Grossman 1996; El Goresy et al. 2002). Reaction of perovskite with a liquid followed by subsolidus equilibrium between fassaite and perovskite was proposed to explain the occurrence and mineral chemistry of the Sc-rich fassaites in Efremovka 101.1 (El Goresy et al. 2002). However, this model cannot be applied to the Sc-rich grain in NQW3–9, since it is isolated in melilite and distant from any available perovskites (Fig. 1d). On the other hand, the fassaite rims on perovskite in the same CAI are Sc_2O_3-poor. Furthermore, the distinct Sc_2O_3/ZrO_2 ratios between the Sc-fassaite and the fassaite rims argue against a similar origin. Although reported Sc_2O_3/ZrO_2 ratios of Sc-rich fassaites vary widely among CAIs, there is a positive correlation between Sc_2O_3 and ZrO_2 within the individual CAIs (Fig. 4). This is most evident for fassaite in the Efremovka inclusion 101.1. Although 101.1 has 4 populations of perovskite with a wide range of Sc_2O_3/ZrO_2 ratios, all analyses of the fassaite rims on perovskites have a near constant Sc_2O_3/ZrO_2 ratio (El Goresy et al. 2002). For comparison, the rim of the Sc-fassaite in NQJ3–5–7 contains lower Sc but higher Zr than the core.

Another possibility is that the Sc-fassaite formed by reaction of a pre-existing Sc-oxide or other Sc-rich phase with a CAI melt. Although no such grains have ever been observed in CAIs from Ningqiang, several Sc_2O_3-rich (>25 wt%) and/or ZrO_2-rich (>50 wt%) phases were reported in a spectacular

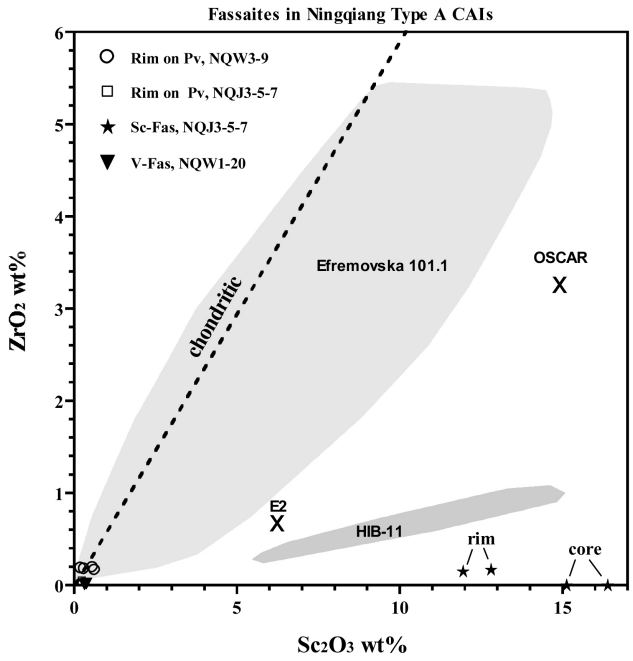

Fig. 4. Sc_2O_3-ZrO_2 plot of fassaites in Ningqiang CAIs. The Sc-fassaite grain in Ningqiang has the highest Sc_2O_3/ZrO_2 ratio, distinct from chondritic and those in other chondrites (El Goresy et al. 2002). Fassaite rims on perovskites near the Sc-rich grain in NQJ3–5–7 are similar to their counterparts in NQW3–9.

blue inclusion that consists of Y-, Zr-rich perovskite and grossite from Acfer 182 (CR) (Bischoff et al. 1993). Alternatively, the Sc-fassaite in NQJ3–5–7 could be a relict, and the Sc-fassaite rims on perovskite in other ultrarefractory CAIs are possible sources. The relict origin is consistent with its occurrence as an inclusion in melilite and its high enrichment of Sc_2O_3, TiO_2, and Al_2O_3. The high Sc_2O_3/ZrO_2 ratio of the Sc-fassaite in NQJ3–5–7 probably reflects a wide range of the ratio among individual CAIs shown in Fig. 4. REE and other trace elements would be helpful to constrain the origin of the Sc-fassaite in NQJ3–5–7, and the analyses are planned.

The coexistence of the Sc-fassaite with the Sc-poor fassaite rims on perovskite indicates that the whole CAI has never been melted. Otherwise, the compositions of these fassaite grains would have been homogenized. This supports a partial melting origin of the CAI as discussed above, based on the presence of the fassaite rims on perovskite.

V-Rich Fassaite

The V-rich fassaite in NQW1–20 occurs as small, euhedral crystals isolated in melilite. No Fremdlinge, magnetite, or metallic Fe-Ni were found in this CAI. This is different from the occurrences of V-rich fassaites reported in other CAIs, which were found in Fremdlinge or coexist with Fe-Ni metal (Armstrong, El Goresy, and Wasserburg 1985; Bischoff and Palme 1987; Caillet and Buseck 1992; El Goresy et al. 2002). V-rich fassaite (up to 6 wt% V_2O_3) has also been found in a Type B CAI, Egg-6, where it occurs as a rim around a large Fe-Ni-V-S-rich opaque assemblage (Meeker, Wasserburg, and Armstrong 1983). These authors suggested that V_2O_3 in the fassaites was derived from the coexisting V-bearing magnetite or Fe-Ni metal during oxidation. However, such a process cannot be applied to the V-rich fassaite in NQW1–20, since it contains no Fremdlinge, magnetite, or Fe-Ni metal. We suggest that the V-rich fassaite grains in NQW1–20 are also relict, probably fragments of pre-existing V-rich fassaite associated with Fremdlinge.

Origins of Ca-Al-Rich Inclusions

Partial Melting of NQW3–9 and NQJ3–5–7

As discussed above, the occurrence of the fassaite rims on perovskite suggests a partial melting origin of both CAIs. Another evidence for annealing or partial melting is the compact texture of melilite. On the other hand, these two inclusions have never been completely melted. This is consistent with their irregular shapes, the presence of the fassaite rims on perovskite, and the coexistence of Sc-fassaite with Sc-poor fassaite rims in NQJ3–5–7. The bulk compositions of NQJ3–5–7, with or without the WL rims, plot close to the range of Type Bs (Fig. 2). If NQJ3–5–7 were completely melted, a crystallization sequence of spinel, melilite, anorthite, and/or fassaite would be expected according to equilibrium crystallization experiments (Stolper 1982). However, no primary anorthite or subliquidus fassaite typical of Type Bs was observed in this inclusion. The absence of anorthite might be related to suppression during non-equilibrium crystallization, but fassaite was expected to crystallize after melilite from an average Type B melt (Stolper and Paque 1986). Furthermore, a complete melting of NQJ3–5–7 will produce a melt with higher concentrations of MgO and SiO_2 in comparison to the typical compact Type As. Melilite that crystallized from the MgO-SiO_2-rich melt is expected to be more åkermanitic than the observation ($Åk_{2–10}$). In fact, melilite in subtype B1 inclusions is typical of zoned ($Åk_{15–60}$) and that in subtype B2s is åkermanitic ($Åk_{60–85}$) (Wark and Lovering 1982). In addition, melilite in two Type B inclusions from Ningqiang also varies from $Åk_{10}$ at the rim to $Åk_{90}$ at the core (Lin and Kimura 2000).

Multi-Stage History of NQW1–20

The spherical shape of NQW1–20 suggests that it may have crystallized from a droplet. The intergrowths of fassaite and spinel inside melilite could be melt inclusions captured during crystallization of the melilite. However, this simple melting origin of NQW1–20 cannot explain the following observations: 1) the melilite in the inclusion is a fragment of a single crystal and shows a ragged outline; 2) the euhedral V-fassaite grains coexist with the assemblages of V-free fassaite + spinel in the melilite; 3) the fassaite-spinel intergrowth assemblages have irregular outlines and voids along boundaries in contact with the melilite (Fig. 1e); and 4) the melilite of NQW1–20 is highly gehlenitic ($Åk_{15–25}$), although its bulk composition plots within the range of Type Bs (Fig. 2).

Another possibility is that the melilite is a relict. This is consistent with its occurrence as a fragment of a single crystal, its gehlenitic composition, and the coexistence of V-rich and V-free fassaites. The depletion of V in the fine-grained fassaite intergrown with spinel cannot be due to the partition of V between these two phases. Although the spinel in NQW1–20 is too small to analyze quantitatively, the grains in both NQW3–9 and NQJ3–5–7 contain V_2O_3 compatible to the coexisting fassaite. In addition, V in the two once-molten Type B inclusions from Ningqiang does not show any evidence for preferring spinel to fassaite (Lin and Kimura 2000). The fine-grained fassaite + spinel intergrowths probably crystallized from a melt, filling voids inside the melilite fragment and covering its surface to form a spherical shape. The melt could be produced by a partial melting of the melilite fragment and other coherent MgO-SiO_2-rich dust. The WL rim of the inclusion probably crystallized from the same liquid but later experienced subsolidus diffusion of Mg and Si from accretionary olivine dust, as proposed by Ruzicka and Boynton (1995) and Wark and Boynton (2001) for WL rims on other CAIs. However, we cannot exclude that these layers condensed continuously on the pre-existing CAI. The repeating sequence of Al-diopside, forsterite, and diopside is

consistent with their narrow condensation temperature range, with diopside condensing a few degrees higher than forsterite (Grossman 1972; Yoneda and Grossman 1995).

As discussed above, V-fassaite in other CAIs always coexists with Fremdlinge, magnetite or metallic Fe-Ni, and V was contributed by diffusion from these phases. However, this is not true for the V-fassaite gains in NQW1–20, because they are isolated in melilite and there are no other V-bearing phases in the neighbor. Furthermore, no evidence suggests that V-rich fassaite condensed from the nebula, since it was not reported in FTAs. The occurrence of the V-fassaite indicates that it predated to the melilite host. We propose that the V-fassaite had a similar origin as those found in other CAIs, then it was incorporated into melilite. This scenario is consistent with the above partial melting origin of the CAI.

CONCLUSIONS

All fassaite rims on perovskite in compact Type A inclusions NQW3–9 and NQJ3–5–7 are characterized by high Ti contents compared with those of other occurrences. The texture and mineral chemistry suggest that these fassaites formed by reaction of perovskite with CAI melts during crystallization. We propose that such rims can be referred to as an indicator of partial melting of Type A inclusions in the nebula.

The Sc-fassaite in NQJ3–5–7 contains the highest Sc_2O_3/ZrO_2 ratio distinct from other Sc-rich fassaites reported in ultrarefractory inclusions. It occurs as a euhedral grain isolated in melilite and shows no apparent relationship with perovskite. The Sc-fassaite could not have formed by a reaction of perovskite as the fassaite rims in the same inclusion did. In addition, V-rich fassaite was found in NQW1–20, which has no observed source of V. We propose that both Sc-fassaite in NQJ3–5–7 and V-rich grains in NQW1–20 are relicts.

Both compact Type A inclusions NQW3–9 and NQJ3–5–7 probably experienced partial melting in the nebula. The refractory spherule NQW1–20 shows a multi-stage history, including formation of the V-fassaite, incorporation of the V-fassaite by melilite, partial melting of the melilite fragment with other MgO-SiO_2-rich dust, and then formation of the WL rim.

Acknowledgments–The constructive reviews by Drs. C. Floss, J. Paque, S. Simon, D. Wark, and E. Scott have substantially improved this paper. The authors are grateful to S. Wang for the Ningqiang sample. This study is supported by the Chinese National Science Fund for Distinguished Young Scholars (Grant 40025311) and the Grant-in-Aid for scientific Research from the Japanese Ministry of Education, Science and Culture (Nr 09640562 and Nr 11640473).

Editorial handling—Dr. Edward Scott

REFERENCES

Armstrong J. T., El Goresy A., and Wasserburg G. J. 1985. Willy: A prize noble Ur-Fremdling—Its history and implications for the formation of Fremdlinge and CAI. *Geochimica et Cosmochimica Acta* 49:1001–1022.

Bischoff A. and Palme H. 1987. Composition and mineralogy of refractory-metal-rich assemblages from a Ca-Al rich inclusion in the Allende meteorite. *Geochimica et Cosmochimica Acta* 51: 2733–2748.

Bischoff A., Palme H., Schultz L., Weber D., Weber H. W., and Spettel B. 1993. Acfer 182 and paired samples, iron-rich carbonaceous chondrites: Similarities with ALH 85085 and relationship to CR chondrites. *Geochimica et Cosmochimica Acta* 57:2631–2648.

Caillet C. L. V. and Buseck P. R. 1992. The "White Angel:" A wollastonite-bearing refractory inclusion in the Leoville chondrite (abstract). *Meteoritics* 27:208.

Davis A. M. 1984. A scandalously refractory inclusion in Ornans (abstract). *Meteoritics* 19:214.

El Goresy A., Palme H., Yabuki H., Nagel K., Herrwerth I., and Ramdohr P. 1984. A calcium-aluminum-rich inclusion from the Essebi (CM2) chondrite: Evidence for captured spinel-hibonite spherules and for an ultra-refractory rimming sequence. *Geochimica et Cosmochimica Acta* 48:2283–2298.

El Goresy A., Zinner E., Matsunami S., Palme H., Spettel B., Lin Y., and Nazarov M. 2002. Efremovka 101.1: A CAI with ultrarefractory REE patterns and enormous enrichments of Sc, Zr, and Y in fassaite and perovskite. *Geochimica et Cosmochimica Acta* 66:1459–1491.

Fuchs L. H. 1971. Occurrence of wollastonite, rhoenite, and andradite in the Allende meteorite. *American Mineralogist* 56: 2053–2068.

Grossman L. 1972. Condensation in the primitive solar nebula. *Geochimica et Cosmochimica Acta* 36:597–619.

Grossman L. 1975. Petrography and mineral chemistry of Ca-rich inclusions in the Allende meteorite. *Geochimica et Cosmochimica Acta* 39:433–454.

Grossman L., Ebel D. S., Simon S. B., Davis A. M., Richter F. M., and Parasad N. M. 2000. Major element chemical and isotopic compositions of refractory inclusions in C3 chondrites: The separate roles of condensation and evaporation. *Geochimica et Cosmochimica Acta* 64:2879–2894.

Kallemeyn G. W. 1996. The classificational wanderings of the Ningqiang chondrite (abstract). 27th Lunar and Planetary Science Conference. pp. 635–636.

Kallemeyn G. W., Rubin A. E., and Wasson J. T. 1991. The compositional classification of chondrites: V. The Karoonda (CK) group of carbonaceous chondrites. *Geochimica et Cosmochimica Acta* 55:881–892.

Kimura M., Noguchi T., Lin Y., and Wang D. 1997. Petrology and mineralogy of an unusual Ningqiang carbonaceous chondrite. In *Geochemical studies on synthetic and natural rock systems*, edited by Gupta A. K., Onuma K., and Arima M. New Delhi: Allied Publishers LTD. pp. 153–165.

Lin Y. and Kimura M. 1997. Titanium-rich oxides bearing plagioclase-olivine inclusions in the unusual Ningqiang carbonaceous chondrite. *Antarctic Meteorite Research* 10:227–248.

Lin Y. and Kimura M. 1998. Anorthite-spinel-rich inclusions in the Ningqiang carbonaceous chondrite: Genetic links with Types A and C inclusions. *Meteoritics & Planetary Science* 33:435–446.

Lin Y. and Kimura M. 2000. Two unusual Type B refractory inclusions in the Ningqiang carbonaceous chondrite: Evidence for relicts, xenoliths, and multi-heating. *Geochimica et*

Cosmochimica Acta 64:4031–4047.

Lin Y. and Kimura M. Forthcoming. Ca-Al-rich Inclusions from the Ningqiang meteorite: Continuous assemblages of the nebular condensates and genetic link to Type Bs. *Geochimica et Cosmochimica Acta*.

Lin Y., Kimura M., and Wang D. 1996. Refractory inclusions in the Ningqiang carbonaceous chondrite (abstract). *Antarctic Meteorites* 21:87–89.

MacPherson G. J. and Grossman L. 1981. A once-molten, coarse-grained, Ca-rich inclusion in Allende. *Earth and Planetary Science Letters* 52:16–24.

MacPherson G. J. and Grossman L. 1984. "Fluffy" Type A Ca-, Al-rich inclusions in the Allende meteorite. *Geochimica et Cosmochimica Acta* 48:29–46.

Meeker G. P., Wasserburg G. J., and Armstrong J. T. 1983. Replacement textures in CAI and implications regarding planetary metamorphism. *Geochimica et Cosmochimica Acta* 47: 707–721.

Nazarov M. A., Patchen A., and Taylor L. A. 2000. Rhonite-bearing Ca, Al-rich inclusions of the Efremovka (CV3) chondrite (abstract). 31st Lunar and Planetary Science Conference. p. 1242.

Podosek F. A., Zinner E. K., MacPherson G. J., Lundberg L. L., Brannon J. C., and Fahey A. J. 1991. Correlated study of initial $^{87}Sr/^{86}Sr$ and Al/Mg isotopic systematics and petrologic properties in a suite of refractory inclusions from the Allende meteorite. *Geochimica et Cosmochimica Acta* 55:1083–1110.

Rubin A. E., Wang D., Kallemeyn G. W., and Wasson J. T. 1988. The Ningqiang meteorite: Classification and petrology of an anomalous CV chondrite. *Meteoritics* 23:13–23.

Ruzicka A. and Boynton W. V. 1995. Quantitative models of CAI rim layer growth (abstract). *Meteoritics* 30:570.

Simon S. B., Grossman L., and Davis A. M. 1991. Fassaite composition trends during crystallization of Allende Type B refractory inclusion melts. *Geochimica et Cosmochimica Acta* 55:2635–2655.

Simon S. B., Davis A. M., and Grossman L. 1996. A unique ultrarefractory inclusion from the Murchison meteorite. *Meteoritics & Planetary Science* 31:106–115.

Simon S. B., Davis A. M., and Grossman L. 1998. Formation of an unusual compact type A refractory inclusion from Allende. *Meteoritics & Planetary Science* 33:115–126.

Simon S. B., Davis A. M., and Grossman L. 1999. Origin of compact type A refractory inclusions from CV3 carbonaceous chondrites. *Geochimica et Cosmochimica Acta* 63: 1233–1248.

Stolper E. 1982. Crystallization sequences of Ca-Al-rich inclusions from Allende: An experimental study. *Geochimica et Cosmochimica Acta* 46:2159–2180.

Stolper E. and Paque J. M. 1986. Crystallization sequences of Ca-Al-rich inclusions from Allende: The effects of cooling rate and maximum temperature. *Geochimica et Cosmochimica Acta* 50: 1785–1806.

Sylvester P. J., Simon S. B., and Grossman L. 1993. Refractory inclusions from the Leoville, Efremovka, and Vigarano C3V chondrites: Major element differences between Types A and B, and extraordinary refractory siderophile element compositions. *Geochimica et Cosmochimica Acta* 57:3763–3784.

Ulyanov A. A., Korina M. I., Nazarov M. A., and Sherbovsky E. Y. 1982. Efremovka CAIs: Mineralogical and petrological data (abstract). 13th Lunar and Planetary Science Conferencs. pp. 813–814.

Wark D. A. 1987. Plagioclase-rich inclusions in carbonaceous chondrite meteorites: Liquid condensates? *Geochimica et Cosmochimica Acta* 51:221–242.

Wark D. and Boynton W. V. 2001. The formation of rims on calcium-aluminum-rich inclusions: Step I—Flash heating. *Meteoritics & Planetary Science* 36:1135–1166.

Wark D. A. and Lovering J. F. 1982. The nature and origin of type B1 and B2 Ca-Al-rich inclusions in the Allende meteorite. *Geochimica et Cosmochimica Acta* 46:2581–2594.

Yoneda S. and Grossman L. 1995. Condensation of CaO-MgO-Al_2O_3-SiO_2 liquids from cosmic gases. *Geochimica et Cosmochimica Acta* 59:3413–3444.